

# Frequency-domain photothermoacoustics: Alternative imaging modality of biological tissues

Sergey Telenkov, Andreas Mandelis,<sup>a)</sup> Bahman Lashkari, and Michael Forcht

*Department of Mechanical and Industrial Engineering, Centre for Advanced Diffusion-Wave Technologies (CADIFT), University of Toronto, Toronto M5S 3G8, Canada*

(Received 10 May 2008; accepted 5 September 2008; published online 19 May 2009)

Frequency-domain photothermoacoustic (FD-PTA) imaging of biological tissues is presented and compared with the conventional time-domain methodology. We demonstrate that tissue imaging can be performed with high axial resolution without the necessity to employ short-pulse and high peak-power laser systems to generate acoustic transients. The presented analysis shows that depth information in the FD-PTA method can be recovered by using linear frequency-modulated (chirped) optical excitation and frequency-domain signal processing algorithms. The signal-to-noise ratio can be increased significantly using correlation processing, which can compensate for the small amplitude of acoustic waves typical to the periodic excitation mode. Additionally, narrow-band signal demodulation enables depth-specific and confocal tissue imaging using the optically induced photothermoacoustic effect. Application of the FD-PTA is demonstrated in experiments with turbid phantoms and *ex vivo* tissue specimens. © 2009 American Institute of Physics.

[DOI: [10.1063/1.3116136](https://doi.org/10.1063/1.3116136)]

## I. INTRODUCTION

Development of noninvasive optical imaging modalities has been the subject of intense interest for decades in a quest for cost-effective, sensitive, and safe screening techniques to assist in medical diagnostics and therapies.<sup>1</sup> This interest was stimulated in part by the potential for quantitative evaluation of tissue optical properties that can be linked to physiological activity and the possibility to detect disease at early stages of progression. The term “optical” in the context of biomedical imaging applications is applied quite broadly covering spectral ranges from microwave radiation to UV; however, significant effort is focused in the near-IR region (700–1000 nm) where the so-called “optical window” allows relatively deep penetration of electromagnetic radiation in the tissue. Among numerous biological substances identified in the near-IR, optical contrast due to blood hemoglobin is very important because the degree of hemoglobin oxygenation is directly related to functional activity, which opens the possibility of functional imaging as opposed to anatomical information provided by other means such as x-ray or ultrasound imaging. One of the most serious challenges any purely optical technique must deal with is related to strong light scattering. Since the typical mean free path of near-IR photons is about 1 mm in the tissue, optical imaging of deep structures must rely on light subjected to multiple scattering events prior to reaching a photodetector. Although significant progress has been achieved in the development of diffuse optical tomography,<sup>2,3</sup> optical methods suffer from low spatial resolution and poor image quality. On the other hand, optical modalities utilizing ballistic and near-ballistic photons (optical coherence tomography<sup>4</sup> and time-gated techniques<sup>5,6</sup>) are more suited for imaging of low-scattering media (ocular tissues) or thin tissue layers.

To alleviate difficulties affecting the performance of optical imaging modalities, various alternative and hybrid techniques have been under active development in the past two decades. Among such techniques, photoacoustic imaging is emerging as a very promising modality, which offers sensitivity to optical contrast similar to diffuse optical tomography combined with relatively high spatial resolution typical of ultrasonic imaging. Since the physical process responsible for generation of mechanical deformations is primarily thermoelastic, this technique is also referred to as photothermoacoustic (PTA) imaging to underscore the chain of energy conversion. Although the thermal nature of acoustic sources usually is not mentioned explicitly, the PTA terminology is justified because it takes into account conditions when heat conduction cannot be neglected, for example, when long optical exposure is used and/or the thermal conductivity of test samples is high. From the viewpoint of biomedical applications, the PTA method provides a means of probing optical contrast in the tissue by acoustic waves generated as a result of thermoelastic effects that occur in light absorbing structures (chromophores). Since acoustic scattering in tissue is approximately two orders of magnitude lower<sup>7</sup> than optical scattering, it is possible to image the tissue at depths of several centimeters without significant loss of spatial resolution, provided the sensitivity of the associated ultrasonic transducers is adequate for detection of weak pressure waves.<sup>8,9</sup> The range of biomedical applications where PTA imaging may provide valuable information was given in a recent review<sup>10</sup> by Xu and Wang. Particular attention is focused on several applications including breast cancer detection, brain, and small animal imaging.<sup>11–14</sup>

In the present paper, we review the physics and methodology of conventional time-domain PTA imaging and provide detailed descriptions of the alternative technique based on frequency-domain photothermoacoustics (FD-PTAs) re-

<sup>a)</sup>Electronic mail: [mandelis@mie.utoronto.ca](mailto:mandelis@mie.utoronto.ca).

ported in our earlier studies.<sup>15–17</sup> We highlight the differences between the two imaging modalities and present basic signal processing algorithms that can be utilized to take advantage of specific features provided by the frequency-domain method. We demonstrate that the concept of FD-PTA imaging with a linear frequency-modulated (LFM) optical source provides depth information similar to the time-of-flight measurements of conventional time-domain photoacoustics, but in addition it allows the use of frequency-domain signal processing methods to increase signal-to-noise ratio (SNR). The characteristics of the FD-PTA imaging method and the relevant signal processing algorithms are discussed and demonstrated in experiments with turbid phantoms and tissue samples *ex-vivo*.

## II. TWO MODALITIES OF PTA IMAGING

The PTA imaging of biological tissues relies on acoustic waves generated as a result of the thermoelastic effect stimulated by inhomogeneous absorption of electromagnetic energy. The near-IR spectral range has been traditionally used to probe deep tissue structures because optical radiation can penetrate down to a significant distance below the surface and many important tissue chromophores such as hemoglobin have distinct absorption spectra. The possibility of non-invasive measurements of tissue optical properties is stimulating the rapid development of PTA technologies. The broad scope of PTA studies can be categorized and labeled according to the mode of optical excitation of test specimens. Acoustic waves can be generated either by short (nanosecond) optical pulses with high peak power or by a continuously modulated optical source with relatively low mean power and high modulation frequency.<sup>18</sup> The former technique emerged over the years as a preferable way of producing large-magnitude acoustic transients and a number of numerical algorithms have been developed for tomographic imaging of subsurface chromophores.<sup>19–21</sup> The latter technique was originally employed in the discovery of the photoacoustic effect and has been utilized frequently in spectroscopic studies.<sup>22,23</sup> Regardless of the method of optical excitation, the characterization of tissue optical properties by PTA phenomena is a multistage analysis involving modeling of photon transport in highly scattering media, heat conduction processes, and elastic wave generation. Moreover, the physical nature of these phenomena in biological materials often requires complete three-dimensional (3D) analysis applied to test samples with complicated geometrical shapes. The specifics of optical interaction and tissue photothermal properties can be utilized to simplify the problem. It is natural to assume that the relatively slow heat conduction of a tissue does not affect the spatial extent of the photogeneration region when nanosecond optical pulses are used or acoustic waves are generated in the megahertz frequency range. This (adiabatic) assumption of thermal confinement ignores heat conduction and monitors the position of acoustic sources via their optical absorption coefficient, thereby relating the characteristics of the acoustic response to the optical properties of the tissue. The almost universal reference to the pulsed mode as “photoacoustics” or “optoacous-

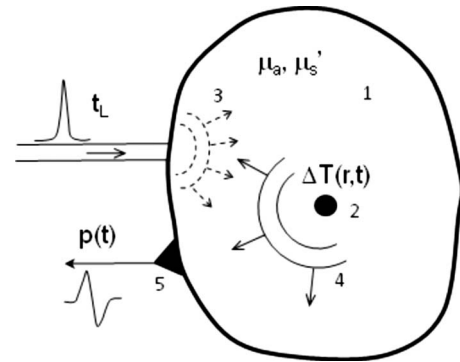


FIG. 1. Schematics of the time-domain PTA imaging.  $\mu_a$  and  $\mu'_s$  stand for the optical absorption and reduced scattering coefficient.  $\Delta T(\mathbf{r}, t)$  is the temperature rise as a result of optical absorption and  $p(t)$  is the thermoelastic pressure transient on the surface of the sample.

tics” denotes fast optical excitation, which does not result in appreciable thermal transport following thermoelastic generation.

### A. Conventional time-domain PTA imaging

The principles of the pulsed PTA method are shown schematically in Fig. 1, which depicts a test sample (1) with homogeneous optical parameters ( $\mu_a, \mu'_s$ ) and an internal inclusion (2) with elevated optical absorption coefficient. The pulsed laser irradiation (3) diffuses in all directions creating nearly uniform optical fluence, which in turn produces a small temperature increase  $\Delta T(\mathbf{r}, t)$ , followed by thermoelastic expansion that generates a transient acoustic pressure (4) detected by an ultrasonic transducer (5). The ultrasonic transducer may be positioned on the same surface as in Fig. 1 (back-propagation mode) or at the opposite surface if available (forward propagation or transmission mode).<sup>24</sup> 90° source-transducer configurations are used for tissue imaging as well.<sup>25</sup> An analytical description of the photoacoustic response is given by the wave equation for pressure  $p(\mathbf{r}, t)$ ,

$$\nabla^2 p(\mathbf{r}, t) - \frac{1}{c_a^2} \frac{\partial^2 p(\mathbf{r}, t)}{\partial t^2} = - \frac{\beta}{C_p} \frac{\partial}{\partial t} q(\mathbf{r}, t), \quad (1)$$

where  $c_a$  is the speed of sound in tissue,  $\beta$  is the isobaric volume thermal expansion coefficient, and  $C_p$  is the specific heat at constant pressure. The source function  $q(\mathbf{r}, t)$  in Eq. (1) is the density of optical energy per unit time deposited at position  $\mathbf{r}$ . The general solution is given by an integral of Green’s function and the source function  $q$  over the spatial domain of distributed sources, which for a 3D unbounded space is given by

$$p(\mathbf{r}, t) = \frac{\beta}{4\pi C_p} \int_V \frac{\frac{\partial}{\partial t} q\left(\mathbf{r}, t - \frac{|\mathbf{r} - \mathbf{r}'|}{c_a}\right)}{|\mathbf{r} - \mathbf{r}'|} d^3 \mathbf{r}'. \quad (2)$$

If exposure to optical irradiation is short, thermalization of the absorbed optical energy results in instantaneous stress buildup within the area of light deposition (stress confinement) and the acoustic pressure can be expressed as

$$p_0(\mathbf{r}) = \Gamma \mu_a(\mathbf{r}) E(\mathbf{r}) = \Gamma H(\mathbf{r}), \quad (3)$$

where the Gruneisen coefficient ( $\Gamma$ ) is a combination of thermoacoustic parameters of condensed media ( $\Gamma=0.1$  for water). The local optical absorption coefficient  $\mu_a(\mathbf{r})$  and the optical fluence  $E(\mathbf{r})$  can be combined into the volumetric energy deposition function  $H(\mathbf{r})$ . Using Eq. (3) as an initial condition for the homogeneous wave equation, the solution can be expressed in the form of a Poisson integral,<sup>26</sup> which has been utilized for the development reconstruction algorithms.<sup>27</sup> The objective of pulsed PTA tomography is the reconstruction of the function  $H(\mathbf{r})$  from multiple-view measurements of acoustic transients and computation of the most probable source distribution minimizing a specific mismatch parameter. In order to determine the optical absorption coefficient  $\mu_a(\mathbf{r})$ , a PTA reconstruction algorithm must also include an adequate model of photon transport in the tissue to provide an independent estimate of optical fluence. Although the profile of acoustic transients generated by Dirac's  $\delta$ -like optical pulses can be used to evaluate the absorption coefficient from Eq. (3), the low SNR and signal distortion due to long propagation distances render such measurements inaccurate.

To estimate the level of acoustic pressure that is detected in pulsed PTA experiments, we consider a small spherical inclusion with radius  $a=5$  mm and absorption coefficient  $\mu_a=1$  cm<sup>-1</sup>, embedded at the depth  $r_s=3$  cm in a tissuelike medium with the effective attenuation coefficient  $\mu_{\text{eff}}=1$  cm<sup>-1</sup>. The initial pressure [Eq. (3)] propagates as a spherical wave with a typical bipolar profile<sup>8</sup> and duration  $2a/c_a=6.6$   $\mu$ s (assuming speed of sound  $c_a=1.5 \times 10^3$  cm/s). Because of light diffusion, the surface irradiation is attenuated in the surrounding tissue approximately by two orders of magnitude. Taking into account that the maximum permissible exposure for skin is 20 mJ/cm<sup>2</sup> in the near-IR, the laser fluence at the 3 cm depth is about 0.2 mJ/cm<sup>2</sup>. Then, the peak pressure reaching a point transducer at the tissue surface ( $\mathbf{r}=\mathbf{r}_d$ ) is

$$p(\mathbf{r}=\mathbf{r}_d) = \frac{\Gamma \mu_a a E(\mathbf{r}_s)}{2|\mathbf{r}_s - \mathbf{r}_d|} = 1.6 \text{ Pa}. \quad (4)$$

Surrounding tissues may also absorb diffuse photons and contribute to the overall PTA response as a low-frequency background signal. Although the background light absorption is usually much smaller, tissue layers near the irradiated surface receive a much greater fraction of optical energy, resulting in large amplitude pressure waves. For example, in a sample with absorption contrast  $\mu_a^{(\text{inc})}/\mu_a^{(\text{tissue})}=10$ , the peak pressure generated near the surface will be  $p \sim 200$  Pa. These simple estimates show that the acoustic signal from a tissue sample will inevitably contain contributions from the subsurface inclusion and a much stronger component originating from tissue superficial layers. This problem becomes increasingly important for the back-propagation imaging mode and specifically for PTA microscopic studies since targeted chromophores are positioned near the irradiated surface. To reduce the effect of near-surface heating, various dark-field illumination methods have been designed.<sup>28</sup> In pulsed PTA tomography, the unwanted background signal

may complicate the reconstruction algorithm and obscure the signal generated at a subsurface inclusion. A number of signal conditioning strategies have been devised to extract signals from subsurface structures in the presence of strong background component.<sup>29</sup>

The minimum detectable size of an inclusion and the maximum imaging depth achieved in PTA measurements are crucial parameters that ultimately define the range of applications where this modality can be successfully employed. With respect to imaging depth, it is important to distinguish between the depths of targeted tissues relative to the irradiated surface and the depth as the distance from the target to the ultrasonic transducer. In the back-propagation mode, there is no difference since the same surface is used for optical excitation and acoustic detection. However, in experiments with large azimuthal separation between optical source and acoustic detector the difference can be substantial. Inasmuch as the optically induced temperature increase and the resulting pressure are proportional to the local optical fluence, the major problem for PTA imaging of deep structures is the delivery of sufficient number of near-IR photons through layers of highly scattering media such as human tissue. On the other hand, attenuation of acoustic waves with frequencies of 1–10 MHz is relatively small and the depth of the target relative to transducer is not an issue, as conventional ultrasonic imaging clearly demonstrates. Therefore, it is important to characterize various PTA modalities and algorithms with respect to the maximum imaging depth achieved away from the optical source. Theoretical estimates based on transducer sensitivity and noise characteristics of the detection instrumentation show the possibility of detecting a 5 mm diameter inclusion in breastlike tissue as deep as 6 cm,<sup>8,11</sup> however experimental evidence is still inconclusive. Results obtained in experiments with phantoms demonstrate acoustic transients arriving from depths exceeding 4 cm,<sup>30</sup> but available *in-vivo* studies reveal difficulties of imaging breast tissue deeper than 2 cm.<sup>31–33</sup> Recent advances in nanoparticle technology and better understanding of light interaction with contrast agents<sup>34,35</sup> may provide significant improvements in PTA imaging and increase imaging depth. An alternative approach to imaging of biomaterials that has not been fully explored utilizes frequency-domain methodologies of acoustic wave generation and signal processing.

## B. Frequency-domain PTA imaging with a linear frequency-modulated optical source

Application of periodically modulated laser sources for generation of acoustic waves is primarily employed in photoacoustic spectroscopy (PAS).<sup>22,23</sup> The theory of PAS was developed in several pioneering works in this field<sup>36–38</sup> and the technique has emerged as a valuable tool for chemical analysis of materials. Spectroscopic terminology frequently utilizes the concept of photoacoustic spectrum to describe the amplitude of acoustic waves generated by photons of different optical frequencies emitted by a polychromatic optical source. Our use of the PTA spectrum is different and implies dependence of acoustic signal on the modulation frequency of monochromatic optical radiation, which is directly related to the time-domain description by a pair of Fourier

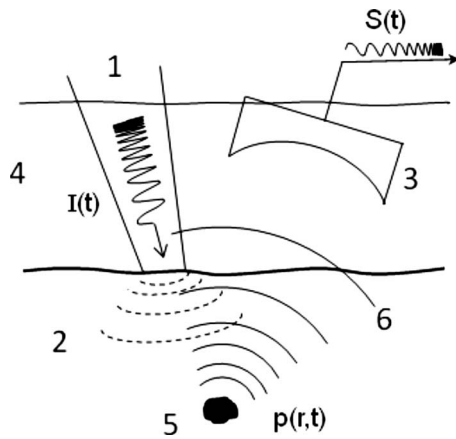


FIG. 2. Diagram of the frequency-domain PTA imaging setup.

transforms. Beyond the spectroscopic analysis of materials, it is problematic to use single frequency PTA with acoustic wavelengths about 1 mm for noninvasive imaging of tissues at depths of several centimeters. While propagation distance is not an issue for harmonic sound waves, the depth information is lost for narrow-band signals. In order to facilitate depth-selective imaging and take advantage of the superior SNR of coherent signal processing methods, we introduced FD-PTA with frequency-swept (chirped) optical excitation.<sup>15–17</sup> Valuable properties of frequency-modulated signals were recognized and utilized long time ago in the design of radar and sonar systems as a convenient way to optimize the tradeoff between the limited power of transmitters and the requirement of high resolution at large detection distances.<sup>39,40</sup> Substantial amount of work on signal processing techniques is available in those fields and the development of FD-PTA technology can benefit from these results. To a certain extent the FD-PTA technology can be called the “PTA sonar” with the only difference that there is no launched wave and returned echo. Instead, materials are probed optically while information is transmitted via acoustic waves following thermoelastic energy conversion.

The experimental setup of frequency-domain PTA is similar to that utilized in time-domain studies. A schematic diagram of the FD-PTA technique for back-propagation imaging mode is shown in Fig. 2.

The key difference with Fig. 1 is the laser source (1) that irradiates the tissue surface (2) with a continuous train of optical chirps, each of duration  $T_{\text{ch}}$ . The time duration  $T_{\text{ch}}$  is an important parameter for processing the received signal and can be relatively long compared to the pulsed laser exposure. Typically,  $T_{\text{ch}}=1$  ms is used, which is selected by weighting various factors such as axial resolution, SNR, processing speed, and amount of computer memory required to acquire multiple scans. To provide acoustic coupling, the ultrasonic transducer (3) and a test sample are immersed in water (4). Acoustic wave (6) detection and imaging of a subsurface inclusion (5) can be done with millimeter lateral resolution by scanning a single focusing transducer parallel to the tissue surface. Instead of a single transducer, a phased array of transducers can be used as well to enable scanning and focusing by programmable beam-forming algorithms.<sup>41</sup> Absorption of laser chirps by subsurface chromophores re-

sults in the generation of frequency-modulated acoustic waves propagating in the tissue. The analytical description of periodic and frequency-modulated PTA generation is most conveniently formulated in the frequency domain utilizing Fourier transforms. Assuming that the time-dependent source function is expressed as  $q(\mathbf{r}, t) = \tilde{q}(\mathbf{r}, \omega)e^{i\omega t}$ , the wave [Eq. (1)] is transformed into an inhomogeneous Helmholtz equation for the spectrum of excited pressure waves

$$\nabla^2 \tilde{p}(\mathbf{r}, \omega) + k^2 \tilde{p}(\mathbf{r}, \omega) = -\frac{i\omega\beta}{C_p} \tilde{q}(\mathbf{r}, \omega), \quad (5)$$

where  $k = \omega/c_a$  is the acoustic wave number and  $\tilde{p}(\mathbf{r}, \omega)$  is the Fourier transform of the acoustic pressure  $p(\mathbf{r}, t)$ . The Green-function solution for unbounded media is given by

$$\tilde{p}(\mathbf{r}, \omega) = -\frac{i\omega\beta}{4\pi C_p} \int_V \frac{e^{ik|\mathbf{r}-\mathbf{r}'|}}{|\mathbf{r}-\mathbf{r}'|} \tilde{q}(\mathbf{r}', \omega) d^3\mathbf{r}'. \quad (6)$$

In general, the divergent spherical pressure wave intercepted by a point transducer at  $\mathbf{r}=\mathbf{r}_d$  can be written as

$$p(\mathbf{r}_d, t) = \frac{|\tilde{p}(\mathbf{r}_s, \omega)|}{4\pi|\mathbf{r}_d-\mathbf{r}_s|} e^{i[\omega(t-|\mathbf{r}_d-\mathbf{r}_s|/c_a)+\theta_a]}, \quad (7)$$

where  $|\tilde{p}(\mathbf{r}_s, \omega)|$  is the pressure amplitude of a point source at  $\mathbf{r}=\mathbf{r}_s$  at angular frequency  $\omega$  and  $\theta_a$  is a phase constant due to thermoelastic conversion. Estimates similar to Eq. (4) for a spherical inclusion in scattering media show that for the safe laser irradiance of 200 mW/cm<sup>2</sup> and modulation frequency of 3 MHz, the amplitude of acoustic pressure at 3 cm distance is  $\sim 2 \times 10^{-3}$  Pa, which is three orders of magnitude less than in the pulsed mode. These estimates demonstrate one of the reasons why pulsed optical sources are generally the preferred way for generating PTA responses. However, frequency-domain methods offer much higher SNR that may compensate for the low signal level. A number of other features specific to the FD-PTA make it a valuable alternative for tissue imaging.

The simplest form of frequency modulation is a linear frequency sweep of the modulating waveform during optical irradiation of a test sample. Consider an optical source with linear frequency modulation corresponding to a sine waveform with quadratic phase variation

$$\theta(t) = \omega_1 t + \frac{b}{2} t^2, \quad (8)$$

where  $\omega_1$  is the starting angular frequency and  $b$  is the frequency sweep rate. According to Eq. (7), the generated acoustic pressure will contain the chirped profile as well. The piezoelectric transducer converts acoustic pressure to a voltage signal  $S(t)$ , which also contains electronic noise. The ultrasonic transducer frequency response function can be taken into account by forming a product of the nearly rectangular spectrum of the acoustic pressure and the transducer frequency response function to obtain the signal spectrum  $\tilde{S}(\omega)$ . It is well known from the theory of radar signals that matched filter processing gives the highest SNR for a known signal hidden in white noise.<sup>40</sup> Mathematically, matched filtering represents correlation processing of a noisy signal

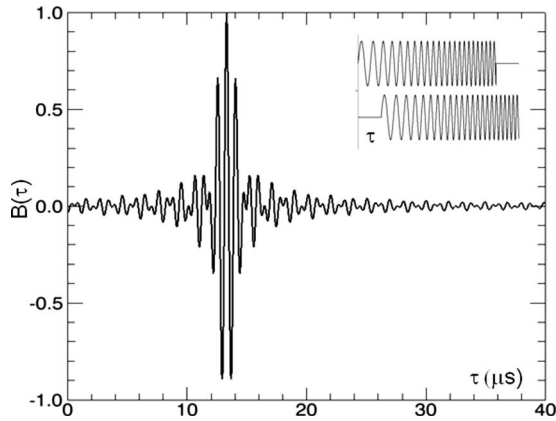


FIG. 3. Autocorrelation function of two chirps with delay time of  $\tau = 13.3 \mu\text{s}$ .

with an exact replica of a signal, the waveform of which is known *a priori*. In case of LFM signals, the autocorrelation function can be derived analytically and is given by

$$B_{\text{LFM}}(t) = \frac{1}{2} S_0^2 \tau_{\text{ch}}^2 \frac{\sin \left[ \frac{\pi m t}{T_{\text{ch}}} \left( 1 - \frac{t}{T_{\text{ch}}} \right) \right]}{\pi m t} \cos(\omega_0 t), \quad (9)$$

where  $S_0$  is the signal amplitude,  $\omega_0 = (\omega_2 - \omega_1)/2$  is the chirp central frequency,  $\omega_2$  is the ending angular frequency, and  $m = bT_{\text{ch}}^2/2\pi$  is the time-bandwidth product. Since an acoustic wave arrives at the ultrasonic transducer with the delay  $\tau = |\mathbf{r}_d - \mathbf{r}_s|/c_a$ , the peak of correlation function (9) will be displaced from the origin by  $t = \tau$ . An example of the correlation function for two LFM chirps of 1 ms long with frequency sweep from 1 to 5 MHz and time delay of one with respect to another of 13.3  $\mu\text{s}$  is shown in Fig. 3. The correlation function has the typical structure of the sinc function with a sharp peak at  $t = \tau$  accompanied by sidelobes and filled with the harmonic carrier at  $\omega = \omega_0$ . The high level of sidelobes is a signal processing artifact, which can be reduced by appropriate windowing of the finite time waveforms at the expense of central peak broadening. The output of the matched filter depends on the input chirp parameters, specifically, the theoretical ratio of amplitudes  $|S_{\text{out}}|/|S_{\text{in}}| = m^{1/2}$  and the signal compression ratio  $T_{\text{ch}}/T_B = m$ . In our experiments,<sup>17</sup> the time-bandwidth product was  $m = 4000$ , which gives an amplitude gain of about 63 and signal compression to 250 ns. The width of correlation function defines the axial resolution achieved with matched filter processing. For speed of sound  $1.5 \times 10^5 \text{ cm/s}$ , the width of 250 ns translates into 375  $\mu\text{m}$  of axial resolution. Additional increase in SNR by a factor of  $N^{1/2}$  can be gained by averaging  $N$  chirps from the continuous sequence received by a transducer. The correlation processing algorithm can be efficiently implemented using signal representation in the Fourier domain and is shown in Fig. 4(a). Typically, the detected acoustic signal is not an exact replica of the stored modulation waveform since the complex amplitude [Eq. (7)] is frequency dependent, but it contains the same frequency spectrum with an additional phase shift  $k \cdot |\mathbf{r}_d - \mathbf{r}_s|$  due to the wave propagation and thermoelastic conversion  $\theta_a$ . When the cross correlation of two signals is computed, the resulting output

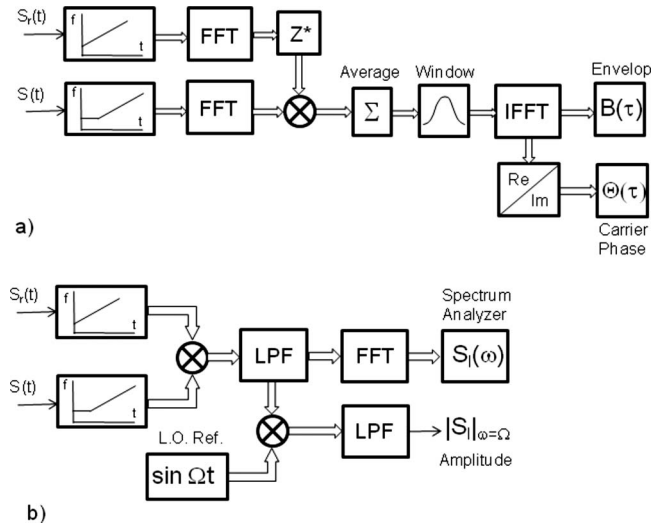


FIG. 4. Block diagram of the signal processing algorithms: (a) frequency-domain cross-correlation processing and (b) spectrum analyzer technique with coherent demodulation.

contains distinct peaks at the time  $\tau = |\mathbf{r}_d - \mathbf{r}_s|/c_a$ , indicating the arrival of the acoustic wave. The uncertainty of the constant phase  $\theta_a$  does not alter the peak position more than  $\pi/\omega_0$  and can be compensated by adjusting the initial phase of the reference chirp. The potential of the correlation processing algorithm for detection of signals masked by strong noise is shown in Fig. 5. These data show the computed cross-correlation amplitude and phase for two software-generated chirps of 1 ms long with delay times of 20 and 60  $\mu\text{s}$ , respectively, and amplitude ratio of 10. The zero-mean Gaussian noise with amplitude much greater than the chirped signals was added (SNR was  $10^{-4}$  for the second chirp). Correlation processing and averaging of 100 signals clearly indicate the presence of both chirps hidden in the noise. The phase of the cross correlation is shown in Fig. 5(b), which was computed with application of threshold filtering to remove spurious fluctuations due to noise. The rapid change in the phase is consistent with Eq. (9), which predicts the linear phase dependence on time ( $\omega_0 t$ ) due to the presence of the harmonic component at the central frequency  $\omega_0$ . The phase data do not provide additional information on the acoustic response but can be useful for suppressing noise in PTA images by a narrow-band filter tuned to  $f_0 = \omega_0/2\pi$ .

Another signal processing method is called the spectrum analyzer technique,<sup>40</sup> which is shown schematically in Fig. 4(b). The result of signal processing is shown in Fig. 6. This method is based on the heterodyne mixing of two LFM signals: the reference chirp  $S_r(t)$  and the PTA signal  $S(t)$  delayed by  $\tau$ . Since both signals have phase dependence given by Eq. (8) with the additional phase shift  $\omega\tau$  in  $S(t)$ , the product of two signals followed by low-pass filtering forms the intermediate frequency signal  $S_f(t)$ , which is

$$S_f(t) = \langle S_r(t) S(t - R/c_a) \rangle = \frac{1}{2} S_0 \cos \left[ b \frac{R}{c_a} t + \theta(R/c_a) \right], \quad (10)$$

where  $S_0$  is the signal amplitude (assuming the reference amplitude  $|S_r| = 1$ ) and  $R = |\mathbf{r}_d - \mathbf{r}_s|$ . Therefore, the heterodyne

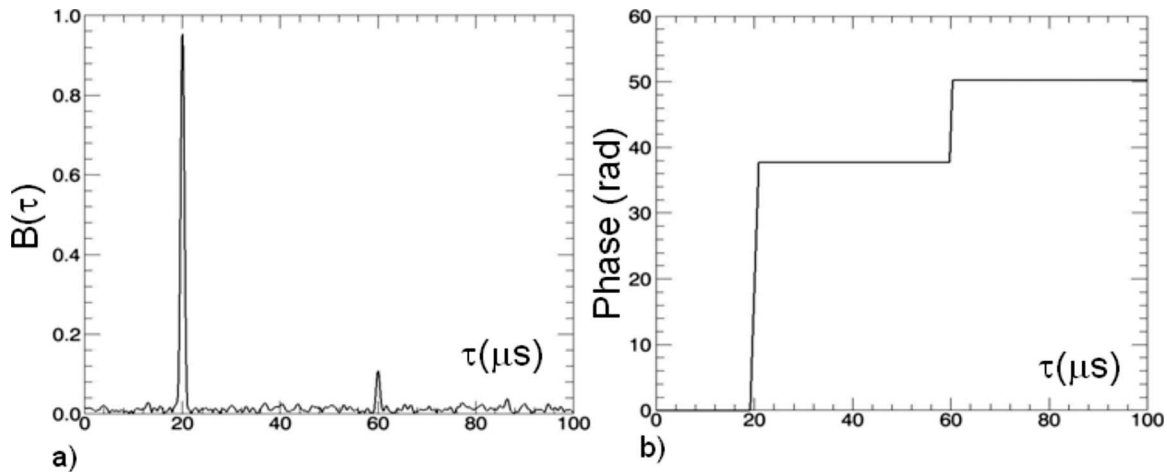


FIG. 5. Signal detection in the presence of strong noise. SNR for the chirp at 60  $\mu\text{s}$  is  $10^{-4}$ .

frequency down conversion creates a signal with constant frequency  $\Omega = bR/c_a$  and duration  $T_{\text{ch}}$ . When acoustic signals arrive from discrete chromophores positioned at different depths, the spectrum of the intermediate signal  $\tilde{S}_I(\omega)$  contains discrete frequency components proportional to the chromophore depths. The heterodyned signal can be examined either by a digital spectrum analyzer or a narrow-band coherent detector with a local reference oscillator tuned to the frequency  $\Omega$ . The chirp waveforms used in our imaging experiments had the sweep rate  $b = 4 \times 10^9$  Hz/s, which, for a chromophore positioned at the depth of 3 cm, corresponds to the intermediate frequency of  $\Omega = 80$  kHz. There are several advantages of using heterodyne mixing for detection of PTA responses. First, this technique offers direct mapping of spatial information into the frequency spectrum of the intermediate signal, which can be examined with high precision in the frequency domain. Second, using narrow-band coherent processing enables depth-selective imaging of tissue. Since narrow-band signal detection allows efficient suppression of contributions from other depths, the strong signal from the irradiated surface can be reduced significantly or

even eliminated. Third, this method enables confocal PTA imaging,<sup>17</sup> provided the depth-selective imaging is conducted with a high numerical aperture focusing ultrasonic transducer. An example of signal processing with the spectrum analyzer technique for the same chirps as in Fig. 5 is shown in Fig. 6, where delay times of 20 and 60  $\mu\text{s}$  result in two discrete frequencies at 80 and 240 kHz, respectively, of the intermediate signal.

### III. EXPERIMENTAL DEMONSTRATION OF FREQUENCY-DOMAIN PTA IMAGING

We demonstrate the application of the FD-PTA method for noninvasive tissue imaging in a series of experimental studies with turbid phantoms and *ex-vivo* chicken breast specimens containing an implanted subsurface inclusion with absorption coefficient greater than the surrounding tissue. Details of the system apparatus employed in these studies were described elsewhere.<sup>17</sup> Laser radiation at the wavelength  $\lambda = 1064$  nm was used to generate PTA signals in the test samples. The continuous-wave (CW) laser beam was modulated by an acousto-optic modulator, which was driven by LFM signals with linear frequency sweep in the range of 1–5 MHz. The modulated laser beam with the mean power of 100–400 mW was focused onto a spot (diameter  $\sim 1$  mm) at the incidence angle of  $\sim 10^\circ$ . To ensure acoustic coupling, the test specimens were immersed in water and the focused ultrasonic transducer (resonant frequency of 3.5 MHz and focusing distance of 25 mm) was aligned with the laser spot on the surface to maximize the signal magnitude. Two-dimensional slice images were created by combining multiple depth scans recorded at various lateral positions along the sample surface. An example of correlation processing in the case of turbid phantoms ( $\mu'_s = 1.3$  cm $^{-1}$ ,  $\mu_a = 0.5$  cm $^{-1}$ ) with subsurface chromophores ( $\mu_a = 4.2$  cm $^{-1}$ ) is shown in Fig. 7. The lineshape of the correlation function was computed for three positions along the surface (labeled as “distance”) and the result shows contributions from the sample-water interface (1), chromophore top surface (2), and echo signal (3). The signal from the sample-water interface (1) in Fig. 7 is strongest because the sample was positioned exactly at the focal distance of the ultrasonic transducer. Fig-

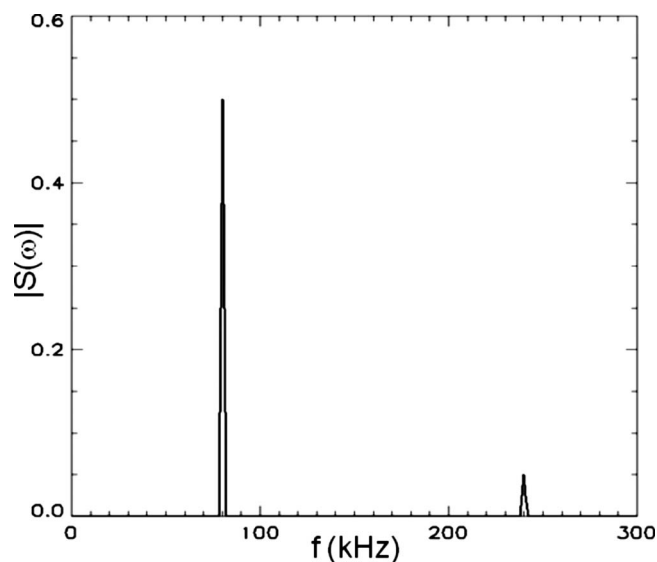


FIG. 6. Result of heterodyne mixing and the spectrum analyzer processing.

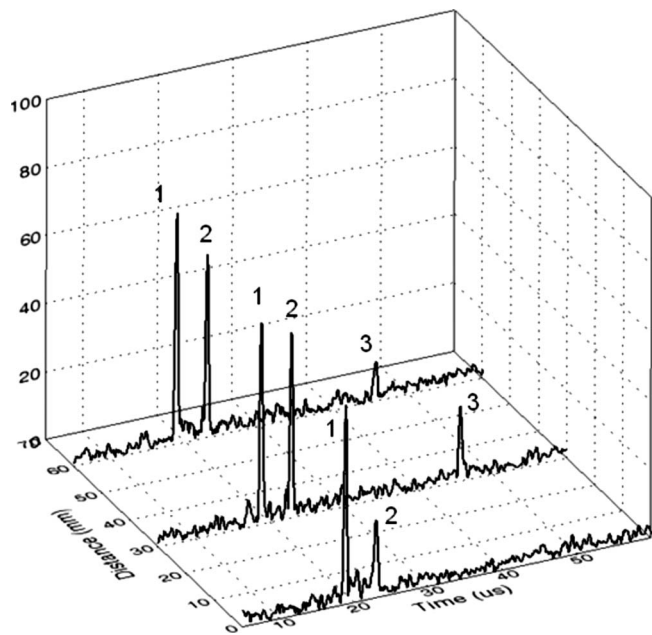


FIG. 7. Cross-correlation function in a phantom sample with subsurface chromophores: (1) signal due to water-sample interface, (2) subsurface inclusion, and (3) reflected signal.

ure 7 shows that it is possible to enhance the signal from subsurface structures by moving the transducer focal point below the surface (along the “time” axis). The result of multiple scans of a chicken breast combined into a single slice image is shown in Fig. 8. The image in Fig. 8(a) was acquired with the surface (A) at the focal distance of the transducer and Fig. 8(b) with the focal spot positioned at the depth of the inclusion (B). The signal (C) is an acoustic reflection of the inclusion from the sample back surface. Increase in contrast of the inclusion in Fig. 8(b) was observed due to better sensitivity in the focal zone.

Imaging of *ex-vivo* tissue was conducted with slabs of a chicken breast and stained polyvinyl chloride (PVC) plastisol as an absorbing inclusion inserted at the depth of 6 mm below the irradiated surface. In these measurements, the ultrasonic transducer was scanned over the area 12 × 12 mm in the horizontal plane and the correlation function was computed at each point of the two-dimensional coordinate array. Combined results produced a 3D volume of correlation am-

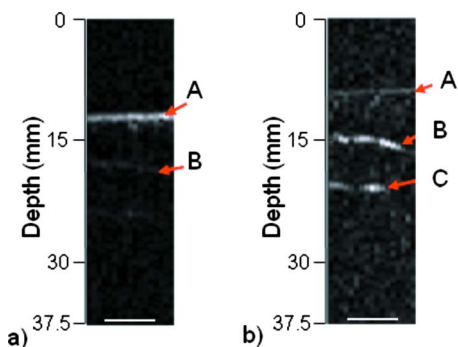


FIG. 8. (Color online) Effect of transducer focal zone position on image contrast (phantom sample): (a) focal zone on the sample surface (b) and (b) focal zone below the surface at the chromophore (b) position. Signal (c) is acoustic reflection. Scale bar=5 mm.

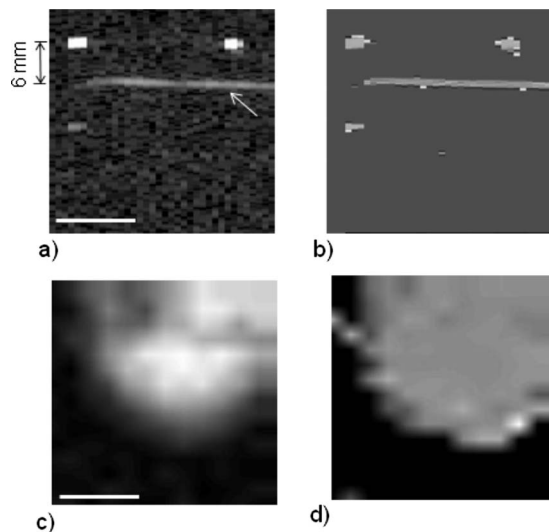


FIG. 9. Correlation imaging of chicken breast using amplitude and phase data (arrow shows inclusion). Cross-sectional images of (a) amplitude and (b) phase derivative  $d\theta/dt$ . Depth-selective imaging with (c) amplitude and (d) phase derivative at the depth of 6 mm. Scale bar=5 mm.

plitude and phase. Since the phase varies linearly at the moments of correlation [Fig. 5(b)], it is more convenient to use the time derivative of the phase  $d\theta/dt$ , which gives the single frequency  $\omega_0$  signal near the peak of correlation and zero otherwise. Images of the correlation amplitude and the phase derivative are shown in Figs. 9(a) and 9(b), respectively. Taking slices of the 3D volume at a fixed delay time, a depth-specific image can be reconstructed. Figures 9(c) and 9(d) show an example of such imaging with the amplitude and the phase derivative at the delay time of 22  $\mu$ s. The images of both amplitude and  $d\theta/dt$  show the round shape of the subsurface inclusion.

Similar to the correlation processing, the spectrum analyzer technique can be used for depth-specific imaging. In this case, the frequency of the local oscillator must be scanned in a predefined range to image the sample at specific depth locations. The results with chicken breast are shown in Fig. 10. In this experiment, the subsurface inclusion ( $\mu_a = 4 \text{ cm}^{-1}$ ) was embedded at 9 mm below the irradiated sur-

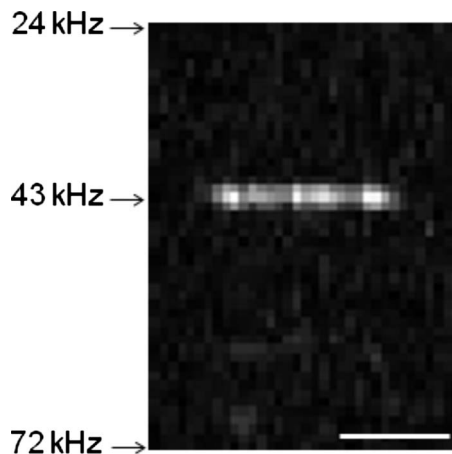


FIG. 10. Imaging of chicken breast using spectrum analyzer technique. Signal at 43 kHz is due to inclusion positioned at 9 mm below the tissue surface.

face and the frequency of the local oscillator was scanned in the range of 24–72 kHz, which corresponds to the scanning distance from the transducer  $c_a\Omega/b=18\text{--}54$  mm ( $b=2\times 10^9$  Hz/s). The top surface of the inclusion appears at 43 kHz (32 mm) while the surface of the chicken breast (not visible) was at 23 mm. Depth-specific imaging is realized by keeping the oscillator frequency fixed during the transducer lateral scan.

#### IV. CONCLUSIONS

The physics of the frequency-domain PTA imaging modality and the differences between FD-PTA and the conventional time-domain method have been presented. We demonstrated that the PTA technique with linear frequency-swept optical modulation can be used as an alternative imaging tool providing a number of valuable features that may improve noninvasive tissue characterization. These features include high SNR of correlation processing without loss of axial resolution, precise control of the imaging depth by frequency selective signal demodulation, narrow-band filtering to reduce signals due to background absorption, and the possibility of confocal microscopic PTA imaging in the back-propagation mode. Despite the small amplitude of the photogenerated acoustic waves, the present FD-PTA system enabled imaging of tissue-like phantoms at the depths exceeding 1 cm. Although the theoretical estimates obtained in the time-domain studies show the possibility of much greater imaging depth, direct comparison to assess the benefits and deficiencies of two modalities under similar experimental conditions is still needed. We believe that improvements in acoustic wave detection (use of phased arrays combined with beam-forming algorithms) and enhancing the PTA generation by contrast agents may extend the imaging depth. Another feature that makes the FD-PTA technology attractive for biomedical applications is a wide selection of low-cost diode lasers that can be used for multiwavelength imaging instead of expensive pulsed optical parametric systems utilized in time-domain measurements. This opens the possibility of molecular-specific imaging with a compact and inexpensive instrumentation.

#### ACKNOWLEDGMENTS

The authors are grateful to the Ministry of Research and Innovation (MRI), Government of Ontario for the 2007 Discovery Award in Science and Engineering to A.M., which made this research possible.

<sup>1</sup>*Handbook of Optical Biomedical Diagnostics*, edited by V. V. Tuchin (SPIE Press, Bellingham, 2002).

<sup>2</sup>S. R. Arridge, *Inverse Probl.* **15**, R41 (1999).

<sup>3</sup>A. P. Gibson, J. C. Hebden, and S. R. Arridge, *Phys. Med. Biol.* **50**, R1 (2005).

<sup>4</sup>D. Huang, E. A. Swanson, C. P. Lin, J. S. Schuman, W. G. Stinson, W. Chang, M. R. Hee, T. Flotte, K. Gregory, C. A. Puliafito, and J. G.

Fujimoto, *Science* **254**, 1178 (1991).

<sup>5</sup>M. R. Hee, J. A. Izzat, J. M. Jacobson, and J. G. Fujimoto, *Opt. Lett.* **18**, 950 (1993).

<sup>6</sup>G. Mitic, J. Kolzer, J. Otto, E. Plies, G. Solkner, and W. Zinth, *Appl. Opt.* **33**, 6699 (1994).

<sup>7</sup>F. A. Duck, *Physical Properties of Tissue* (AP, London, 1990).

<sup>8</sup>A. Oraevsky and A. Karabutov, *Proc. SPIE* **3916**, 228 (2000).

<sup>9</sup>V. G. Andreev, A. A. Karabutov, and A. A. Oraevsky, *IEEE Trans. Ultrason. Ferroelec. Freq. Control* **50**, 1383 (2003).

<sup>10</sup>M. Xu and L. Wang, *Rev. Sci. Instrum.* **77**, 041101 (2006).

<sup>11</sup>S. Ermilov, A. Stein, A. Conjusteau, R. Gharieb, R. Lacewell, T. Miller, S. Thompson, P. Otto, B. McCorvey, T. Khamapirad, M. Leonard, and A. Oraevsky, *Proc. SPIE* **6437**, 643703 (2007).

<sup>12</sup>S. Manohar, A. Kharine, J. C. G. van Hespren, W. Steenbergen, and T. G. van Leeuwen, *Phys. Med. Biol.* **50**, 2543 (2005).

<sup>13</sup>G. Ku, X. Wang, X. Xie, G. Stoica, and L. V. Wang, *Appl. Opt.* **44**, 770 (2005).

<sup>14</sup>E. Z. Zhang, J. Laufer, and P. Beard, *Proc. SPIE* **6437**, 64370S (2007).

<sup>15</sup>Y. Fan, A. Mandelis, G. Spirou, and I. A. Vitkin, *J. Acoust. Soc. Am.* **116**, 3523 (2004).

<sup>16</sup>Y. Fan, A. Mandelis, G. Spirou, I. A. Vitkin, and W. M. Whelan, *Phys. Rev. E* **72**, 051908 (2005).

<sup>17</sup>S. Telenkov and A. Mandelis, *J. Biomed. Opt.* **11**, 044006 (2006).

<sup>18</sup>V. E. Gusev and A. A. Karabutov, *Laser Optoacoustics* (AIP, NY, 1993).

<sup>19</sup>R. A. Kruger, D. R. Reinecke, and G. A. Kruger, *Med. Phys.* **26**, 1832 (1999).

<sup>20</sup>M. Xu, Y. Xu, and L. V. Wang, *IEEE Trans. Biomed. Eng.* **50**, 1086 (2003).

<sup>21</sup>C. G. A. Hoelen and F. F. M. de Mul, *Appl. Opt.* **39**, 5872 (2000).

<sup>22</sup>A. Rosencwaig, *Photoacoustics and Photoacoustic Spectroscopy* (Wiley, New York, 1980).

<sup>23</sup>V. P. Zharov and V. S. Letokhov, *Laser Optoacoustic Spectroscopy* (Springer-Verlag, Berlin, 1986).

<sup>24</sup>A. A. Karabutov, E. V. Savateeva, N. B. Podymova, and A. A. Oraevsky, *J. Appl. Phys.* **87**, 2003 (2000).

<sup>25</sup>S. A. Ermilov, A. Conjusteau, K. Mehta, R. Lacewell, P. M. Henrichs, and A. A. Oraevsky, *Proc. SPIE* **6086**, 608609 (2006).

<sup>26</sup>P. M. Morse and H. Feshbach, *Methods of Theoretical Physics* (McGraw-Hill, New York, 1953).

<sup>27</sup>K. P. Kostli, M. Frenz, H. P. Weber, G. Paltauf, and H. Schmidt-Kloiber, *Appl. Opt.* **40**, 3800 (2001).

<sup>28</sup>K. Maslov, G. Stoica, and L. V. Wang, *Opt. Lett.* **30**, 625 (2005).

<sup>29</sup>V. G. Andreev, A. A. Karabutov, S. V. Solomatina, E. V. Savateeva, V. Aleinikov, Y. V. Zhulina, R. D. Fleming, and A. A. Oraevsky, *Proc. SPIE* **3916**, 36 (2000).

<sup>30</sup>R. O. Esenaliev, H. Alma, F. K. Tittel, and A. A. Oraevsky, *Proc. SPIE* **3254**, 294 (1998).

<sup>31</sup>A. A. Oraevsky, V. A. Andreev, A. A. Karabutov, R. D. Fleming, Z. Gatalica, H. Singh, and R. O. Esenaliev, *Proc. SPIE* **3597**, 352 (1999).

<sup>32</sup>A. A. Oraevsky, A. A. Karabutov, S. V. Solomatina, E. V. Savateeva, V. A. Andreev, Z. Gatalica, H. Singh, and R. D. Fleming, *Proc. SPIE* **4256**, 6 (2001).

<sup>33</sup>T. Khamapirad, P. M. Henrichs, K. Mehta, T. G. Miller, A. T. Yee, and A. A. Oraevsky, *Proc. SPIE* **5697**, 35 (2005).

<sup>34</sup>G. Ku and L. V. Wang, *Opt. Lett.* **30**, 507 (2005).

<sup>35</sup>A. Agrawal, S.-W. Huang, K. C. Day, M. O'Donnell, M. Day, N. Kotov, and S. Ashkenazi, *Proc. SPIE* **6437**, 64370H (2007).

<sup>36</sup>A. Rosencwaig and A. Gersho, *J. Appl. Phys.* **47**, 64 (1976).

<sup>37</sup>A. C. Tam, *Rev. Mod. Phys.* **58**, 381 (1986).

<sup>38</sup>M. W. Sigrist, *J. Appl. Phys.* **60**, R83 (1986).

<sup>39</sup>*Radar Handbook*, edited by M. I. Skolnik (McGraw-Hill, New York, 1990).

<sup>40</sup>C. E. Cook and M. Bernfeld, *Radar Signals. An Introduction to Theory and Application* (Academic, New York, 1967).

<sup>41</sup>R. A. Mucci, *IEEE Trans. Acoust., Speech, Signal Process.* **32**, 548 (1984).